

RESEARCH ARTICLE

Deformable trailing edge flaps for modern megawatt wind turbine controllers using strain gauge sensors

Peter Bjoern Andersen, Lars Henriksen, Mac Gaunaa, Christian Bak and Thomas Buhl

Wind Energy Department, Risø DTU National Laboratory for Sustainable Energy

ABSTRACT

The present work contains a deformable trailing edge flap controller integrated in a numerically simulated modern, variable-speed, pitch-regulated megawatt (MW)-size wind turbine. The aeroservoelastic multi-body code HAWC2 acts as a component in the control loop design. At the core of the proposed controller, all unsteady loads are divided by frequency content. Blade pitching and generator moment react to low-frequency excitations, whereas flaps deal with high-frequency excitations. The present work should be regarded as an investigation into the fatigue load reduction potential when applying trailing edge flaps on a wind turbine blade rather than a conclusive control design with traditional issues like stability and robustness fully investigated. Recent works have shown that the fatigue load reduction by use of trailing edge flaps may be greater than for traditional pitch control methods. By enabling the trailing edge to move independently and quickly along the spanwise position of the blade, local small fluctuations in the aerodynamic forces can be alleviated by deformation of the airfoil flap. Strain gauges are used as input for the flap controller, and the effect of placing strain gauges at various radial positions on the blade is investigated. An optimization routine minimizes blade root fatigue loads. Calculations are based on the 5 MW reference wind turbine part of the UpWind project primarily with a mean turbulent wind speed close to rated power. A fatigue load reduction of 25% in the blade root moment was obtained for a continuous 6.3 m long flap. Copyright © 2009 John Wiley & Sons, Ltd.

KEYWORDS

wind turbine control; deformable trailing edge geometry; strain gauge measurement; optimization

Correspondence

P. B. Andersen, Risø DTU National Laboratory for Sustainable Energy
Wind Energy Division
P.O. Box 49
Frederiksborgvej 399
DK-4000 Roskilde
Denmark
E-mail: pbja@risoe.dtu.dk

Received 13 May 2009; Revised 6 August 2009; Accepted 6 August 2009

1. INTRODUCTION

All wind turbines are subject to unsteady loads. During normal operation, the wind turbine blades will experience fluctuating loads because of the turbulent wind field or the meandering wake deficit from upstream turbines. Yaw conditions, shear flow and tower shadow effect also cause fluctuating loads dependent on the rotational speed. Alleviating these loads can reduce material consumption and thereby turbine weight or increase the lifetime of

the turbine components. Recent work has shown that active load reduction using pitch control for megawatt-size wind turbines can alleviate load increments from yaw errors, wind shear and gusts considerably.^{1,2} Load reduction is realized either by pitching the blades independently (individual pitch) or equally for each blade, but with a phase shift between each blade (cyclic pitch). According to Larsen *et al.*,¹ a comparison to collective pitch, where all blades are pitched equally, shows that cyclic pitch can reduce the blade flap fatigue loads at the hub 21%,

while it can be reduced 25% when using individual pitch. In addition, extreme load on the turbine can be reduced with up to 3% when using cyclic pitch and 6% when using individual pitch for the blade flap at the hub. This means that there is a significant potential in using advanced pitch control for load reduction. However, as wind turbine blades become larger and more flexible, there is an increased need for locally distributed control surfaces.

Adding a flap at the trailing edge to a blade is a well-known method for changing the aerodynamic pressure distribution around the blade. At Risø DTU in Denmark, a continuous research of using trailing edge flaps for reducing load fluctuations on wind turbines has been carried out.^{3–11} Furthermore, efforts in investigating trailing edge devices from trailing edge flap over tabs to jets are being done worldwide. In The Netherlands, the main focus is on trailing edge flaps at Delft University.¹² Delft University conducted a proof concept experiment for ‘smart’ rotor blades.¹³ This experiment showed that loads for periodic disturbances and for turbulence-generated disturbances could be reduced up to 90 and 55%, respectively. Jets are investigated at the Energy Research Center of The Netherlands. In USA, flaps and tabs are being investigated at Sandia National Laboratory in New Mexico and at UC Davis in California.¹⁴ In Greece, at the National Technical University of Athens, a panel code coupled with a free wake vortex particle flow model has been investigated for the purpose of active flap controllers.¹⁵

The flap considered in the present study is not intended as a classic plain flap that rigidly rotates around its hinge point; instead, it is represented by a continuous and smooth deformation of the airfoil trailing edge part, as illustrated in Figure 1, specified through a non-linear deflection shape. This type of flaps was chosen in Risø DTU’s previous work because flow separation, and thereby corresponding noise and drag were reduced, compared to the rigid flap.¹⁶

One way of integrating the flap with the blade at various spanwise positions could be facilitated by the use of valves,

which is illustrated in Figure 2. The proposed valve solution requires additional information about the effect of rotation and hydraulic dynamics in general; however, the present work focuses on locating the optimum radial positions for a given sensor control strategy, and uncover the potential in terms of fatigue load reductions.

Often, state space models provide the foundation in control designs. The state space model can be used in the validation phase or directly to predict and anticipate future events as model predictive controllers. The linearization process is by no means trivial; the interaction between the aerodynamic loading, the elastic deformation, and actuators are highly interdependent. Knowing what dynamics to include and what to throw away is critical. Knowing ‘when’ is another issue; during night times, the wind shear can have a distinct profile, whereas in daytime the profile may have disappeared as the sun heats up the surface causing added turbulence. Instead of writing up a simplified state space model of a turbine for one specific load case for which traditional control tool box utilities can be applied, the presented work utilizes the full-time marching aeroservoelastic multi-body model directly as a component in the control loop design, offering the full palette of parameters for the optimization routine. The downside to this approach is increased computational time. Although control and optimization disciplines are part of the investigation, the presented work primarily aims at uncovering the fatigue load reduction potential for the flapwise blade root moment.

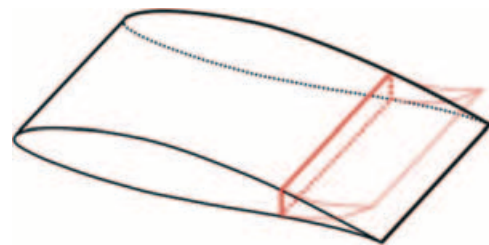


Figure 1. Conceptual design layout of an airfoil section with a deformable trailing edge flap.

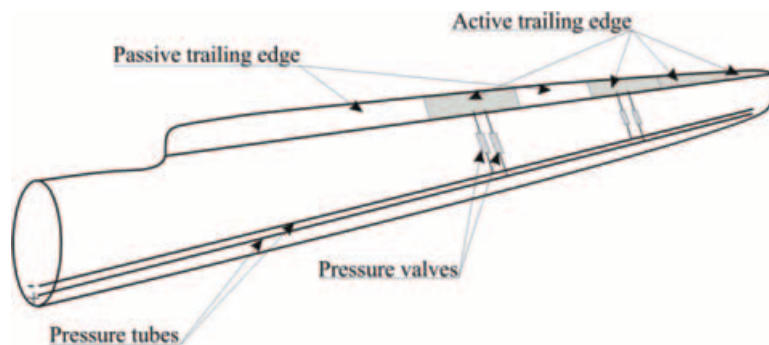


Figure 2. Possible blade design of one blade with trailing edge flaps.

An extended version of the traditional pitch-regulated, variable-speed control algorithm forms the base for the power control. The computations are done for the 5MW reference turbine¹⁷ used in the EU project 'UpWind'.

Results presented in this work are carried out using the aeroelastic code HAWC2.¹⁸ Most of the previous analytical and numerical investigations done on rigid airfoils are based on the potential-flow aerodynamic model from the classical paper by Theodorsen.¹⁹ This includes the aerodynamic effect of a flat trailing edge flap on a flat airfoil. Some of these investigations can be found in Leishman,²⁰ and Hariharan and Leishman.²¹ Other works dealing with deformable camberlines that are not hinged trailing edge flaps have used panel codes²² and even full Navier–Stokes codes,²³ which are more computationally costly models. At Risø DTU, a computationally very efficient unsteady two-dimensional potential-flow model for the aerodynamic forces of a thin airfoil undergoing deformation of the camberline was developed.⁷ Andersen *et al.*^{3,24} extended the model to include viscous effects in the spirit of the Risø version²⁵ of the Beddoes–Leishman-type dynamic stall model.²⁶ The traditional blade element momentum (BEM) models cannot include trailing edge deformations in a direct way; consequently, the near-wake model for trailing vorticity originally proposed by Beddoes²⁷ and investigated by Madsen and Rasmussen²⁸ has been implemented in HAWC2 following the work of Andersen *et al.*²⁹ Subsequently, the aerodynamic part of HAWC2 comprises a near-wake model,²⁹ a dynamic stall model,^{3,24} the far-wake part of a dynamic inflow model,³⁰ a potential tower shadow model and the tip loss correction by Wilson and Lissaman.³¹ The elastic part of HAWC2 includes multi-body Timoshenko finite beam elements. The input model is divided into substructures like tower, nacelle and rotor blades. Each substructure can be divided into a number of bodies which again are divided into finite elements. Unsteady aerodynamic torque, thrust and other loads are calculated.

The setup to be investigated includes an aeroservoelastic code, a generator pitch control, a flap control, parameters for the flap control and a constrained optimization routine.³² The flap control utilizes a high-frequency pass filter and a proportional gain. The flap and strain gauge sensor positions will be varied while calculating the effect in blade root bending moment fatigue numbers. The signal will be distorted with signal noise and signal delays. An oscillating force will be placed on the tower top to test for instabilities using a narrow range of frequencies.

2. MODEL

This section describes the content of the presented work, control algorithm, sensors, flap, optimization strategy and

initial guesses used. The first investigation validates the setup by excluding the elastic part of a wind turbine, and comparing the optimal position to place a flap with simple theory. For the second part, a more detailed investigation is undertaken in which the turbine is elastic. Time lags are added to the strain gauge sensor signal to simulate lags in the control system. Finally, simple time-matching stability analysis of the control system is undertaken by exciting the tower top in lateral and longitudinal directions for a range of harmonic frequencies ranging from 0.1 to 1.0 Hz, and investigating the response.

3. CONTROL ALGORITHM

The flap is an active control device and therefore requires a control algorithm to operate. Numerous control strategies can be applied when designing a closed feedback loop. The control strategy in the present work extends a traditional pitching variable rotor speed (PVRS) power controller specified by Jonkman¹⁷ for the reference 5 MW turbine with a simple flap controller. For the PVRS turbine, the generator moment and blade pitch are controlled using a low-pass filtered rotational rotor speed signal ω_f

$$\tau_\omega \frac{\partial \omega_f}{\partial t} + \omega_f = \omega(t), \quad (1)$$

in which the unfiltered rotational signal is ω , and τ_ω translates to the corner frequency or -3 dB signal drop. Assume deformations are measured as strains ε in distance r_s from the blade root. The proposed strategy in the present work allows the generator and pitch to react to low-frequency rotational rotor speed variations, e.g. because of mean wind speed changes, and the flaps will react to medium- and high-frequency variations from elastic deformations and turbulent gusts. A high-pass filter is therefore part of the flap controller, in which the flap deflection angle β is

$$\beta = K_p [\varepsilon(r_s) - z] \quad (2)$$

$$\tau \frac{\partial z}{\partial t} + z = \varepsilon(r_s) \quad (3)$$

or combining equations (2) and (3) in Laplace domain (complex argument $[s] = [i\omega]$)

$$z = \frac{\varepsilon(r_s)}{\tau s + 1} = \varepsilon(r_s) - \frac{\beta}{K_p} \Leftrightarrow \frac{\beta}{K_p} = \varepsilon(r_s) \left[1 - \frac{1}{\tau s + 1} \right] \quad (4)$$

The proportional gain K_p is the primary control parameter to be determined for the control algorithm.

4. SENSOR

The flap requires some sensor input to operate. The sensor proposed in the present work is strain gauges, but other devices capable of detecting flapwise blade deformations are applicable. By feeding the signal from the strain gauges through the controller to the flaps, the actuation will be lagged in time because of the inertia of the blades. In Buhl *et al.*⁶ and Andersen *et al.*,⁸ (Andersen PB, Henriksen LC, Gaunaa M, Bak C, Buhl T. Deformable trailing edge flaps for modern mega-watt wind turbine controllers using pitot tubes. Unpublished) pitot tubes mounted on the wind turbine blade are used instead, effectively bypassing blade inertia in the actuation loop. Figure 3 illustrates strain gauge sensors and flap actuators used in the present work. As both normal force (N) and bending moment (M) are on hand, a strain gauge-type sensor signal is assumed available at a given spanwise blade position r_s along the finite beam blade elements. A more complex model is needed for simulating strains on a full three-dimensional airfoil with spars and composite plies. The simple beam theory is used in the present work, in which the measured strain ε is given by bending stress σ divided by elastic modulus E for a symmetrically bent beam.

$$\varepsilon = \frac{\sigma}{E} = \frac{N}{AE} - \frac{Mh}{EI}, \quad (5)$$

The normal force N will vary with the rotational rotor speed and depend on blade mass, A is the cross-sectional area, h is the perpendicular distance to the neutral axis and EI is the bending stiffness. Once the location of the strain gauge is chosen, the control system will affect the blade dynamics, making it a fully coupled problem that has to be solved iteratively.

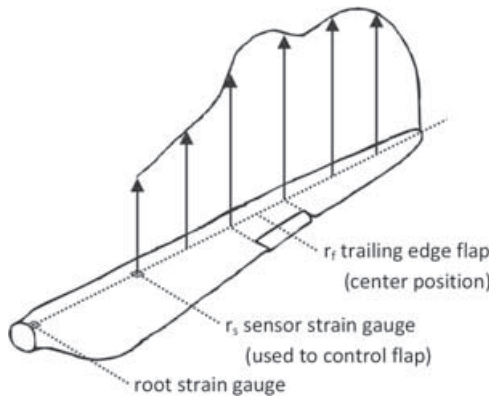


Figure 3. Sensors and flap actuator.

5. FLAP

The chordwise length of the flap is constant 10% of the chord; furthermore, constraints are placed on maximum deflection of $\pm 8^\circ$.

6. OPTIMIZATION STRATEGY

An optimization strategy is needed in order to systematically tune gains and time constants for the proposed controller. The gradient based optimization³² is used for this purpose. Consider a constrained non-linear optimization problem in a form where A and b describe the system of constraints.

$$\begin{aligned} & \text{minimize} && M_x^*(K_p, \tau, r_f, r_s), \\ & \text{subject to} && Ax \leq b, x \geq 0 \end{aligned} \quad (6)$$

The aeroelastic tool HAWC2 will be used to determine the optimization coefficients or gradients by means of a forward finite difference method

$$\frac{\partial M_x^*}{\partial x} = \begin{bmatrix} \frac{\partial M_x^*}{\partial K_p} & \frac{\partial M_x^*}{\partial \tau} & \frac{\partial M_x^*}{\partial r_f} & \frac{\partial M_x^*}{\partial r_s} \end{bmatrix}, \quad (7)$$

where M_x^* is the sum of equivalent blade root moment fatigue load for a given turbulent wind series for all the three blades on the reference turbine, and x is the optimization variable vector containing $[K_p \ \tau \ r_f \ r_s]$. The optimization is by default constrained to

$$A = \begin{bmatrix} r_f & 0 & 0 \\ 0 & r_s & 0 \\ 0 & 0 & \tau \end{bmatrix}, \quad b = \begin{bmatrix} R - 0.5\tilde{l}_f R \\ R \\ 0.4 \frac{\omega_0}{\omega_f} \end{bmatrix}, \quad (8)$$

The strain gauge sensor and flap should not be placed beyond the blade length R . The normalized flap length \tilde{l}_f is constant 10% of R , which is equal to 6.3 m. Finally, initial studies suggested a constraint on the high-pass filter time constant τ , where ω_0 is rated and ω_f is the low-pass filtered rotational rotor speed.

7. INITIAL GUESS

When applying a gradient-based optimization routine to a highly non-linear and possibly non-convex problem, the risk of ending up in local minima exists. Therefore, an effort was made to provide well-suited starting guesses for control gains and filter time constants for the optimization of the gain and filter time constant. After organizing numerous parameter sweeps using HAWC2, two empirical

equations are formulated and given *a posteriori*; they are rooted in the reference 5 MW turbine. A starting guess for a proportional gain K_p is proposed as

$$K_p = \frac{0.02}{\tilde{l}_f} \frac{\sqrt{\omega_b}}{1 + 20\psi^2} \left(\frac{2\omega_0 - \omega}{\tilde{r}} \right)^{1.75} \quad (9)$$

The first flapwise mode shape for the blade (fully clamped) is normalized to unity at maximum deflection; the value ψ represents the mode shape value (between 0 and 1) at radial position \tilde{r} where flap is positioned on the blade; ω_b is the first flapwise eigenfrequency for the reference turbine blade clamped at the blade root. When adjusting the time constant τ , the state variable z will trace sensor ε faster or slower depending on τ , effectively shifting the operational frequency band for the high-pass filter. A simplified equation for finding a good starting guess for the high-frequency pass filter time constant is

$$\tau = 0.045(2\omega_0 - \omega_f)^2 e^{1-\tilde{r}} \quad (10)$$

8. FIRST INVESTIGATION OF A STIFF REFERENCE WIND TURBINE

Numerous parameters can be considered when investigating the fatigue load reduction potential by means of trailing edge flaps mounted on wind turbine blades. Before complex optimizations are performed involving full aero-servoelastic wind turbine simulations, some key features on the behavior on the control authority of trailing edge flaps on rotors may be investigated using simple steady-state engineering approximations. Consider a stiff rotor in an aerodynamic quasi-steady fully attached flow. For constant rotational speed, the steady-state change to the blade root moment caused by variations in local blade loading at radial position r is

$$\Delta M = r\Delta N = rN \frac{\Delta C_N(\beta)}{C_N} = \frac{r}{2} \rho c V^2 \Delta C_N(\beta) \quad (11)$$

An approximate relation for the relative wind speed at rotor radius r , assuming high tip speed ratio, is

$$V \cong r\omega = \tilde{r}R\omega \quad (12)$$

where the rotational rotor speed is ω , and the non-dimensional radial coordinate is expressed as $\tilde{r} = r/R$. The tip speed ratio λ times the free wind V_∞ speed is

$$\lambda V_\infty = \omega R = \frac{V}{\tilde{r}}, \quad (13)$$

which combined yields

$$\Delta M = \frac{1}{2} \rho V_\infty^2 R^2 \lambda^2 \tilde{c} \tilde{r}^3 \Delta C_N(\beta), \quad (14)$$

Again, a tilde signifies non-dimensionalization with the rotor radius R , so non-dimensional chord is $\tilde{c} = c/R$. Neglecting the influence of induction in addition to the assumption of high tip speed ratio, attached flow and constant ratio between length of the flap relative to the length of the chord $\Delta C_N(\beta_{ref}) = \text{const}$. With this in mind, we see that equation (4) contains terms with and without radial dependency. When taking away the terms that are constant throughout the blade changes to the root moment are proportional to non-dimensional blade radius cubed multiplied with non-dimensional chord.

$$\Delta M \propto \tilde{c} \tilde{r}^3 \propto c r^3 \quad (15)$$

The chord usually decreases to zero near the blade tip; therefore, an optimum location for the flap in terms of the authority on root bending moment will depend on the chord distribution for this case.

9. A FULLY ELASTIC WIND TURBINE

Initial studies on an elastic turbine revealed that actuating the flap coupled greatly with torsional, flapwise and somewhat edgewise blade deflections,³³ hence elasticity was included in the present work using HAWC2. On a torsionally stiff blade, deflection of the flap to the pressure surface generates an increase in aerodynamic load, and a deflection to the suction side decreases the aerodynamic load. On a torsionally soft blade, a deflection of the flap toward the pressure surface will create a pitching moment that twists the nose of the blade toward the pressure surface, thereby decreasing the angle of attack and load. For a deflection toward the suction surface, the opposite will happen.

10. EFFECT OF SIGNAL LAG AND DELAY

The strain gauge sensors used in the control design primarily measure the elastic response rather than the actual aerodynamic excitation itself. This type of sensor has the advantage that the aerodynamic force will be correctly integrated as strain well suited for predicting fatigue loads; however, the controller reacts after an aerodynamic loading event has occurred. Other types of delays between event and actuation exist, some are based on choice of equipment, while others on control strategy. Preliminary studies³³ revealed a significant drop in load reduction potential when introducing various time lags in the flap controller. It is therefore deemed important to investigate the effect of having additional signal delays in the controller. Two types of signal delays have been investigated: time lags and time delays. The lag is a simple first-order filter

$$\tau \frac{\partial \varepsilon'}{\partial t} + \varepsilon' = \varepsilon(t) \quad (16)$$

The sensor input to the controller ε' has been filtered from the original signal (t) effectively adding a phase lag and removing the high-frequency content. A signal delay is also investigated in which the signal is placed in a stack and executed some time τ later.

11. EFFECT OF SIGNAL NOISE

Signal noise can be many things, and numerous definitions to signal noise exist. The signal-to-noise ratio (SNR) is well known and can be defined as

$$SNR(dB) = 20 \log \left(\frac{|\varepsilon|}{|\vartheta_\varepsilon|} \right) \tag{17}$$

or signal amplitude divided by the amplitude of the noise (ϑ). The standard deviation of the noise used in the current simulation will scale with the mean of the undisturbed signal as

$$SNR(dB) = 20 \log \left(\frac{\langle \varepsilon \rangle}{\sigma_\vartheta} \right) \tag{18}$$

simply dividing the mean of the signal with the standard deviation of the noise instead, often used in the field of image sensing to describe the SNR. White signal noise with SNR of 1, 2, 3, 4, 5 and 10 dB was investigated, 1 dB being the most deteriorated signal.

12. EXTERNAL TOWER EXCITATION

By observing the fatigue load response in the drivetrain, blade and tower root moments when applying an external tower excitation force, the stability of the flap controller is

investigated. The tower is excited by an oscillating force with constant amplitude and a sweep through different frequencies in both longitudinal and lateral directions. In the simulations used for the results in the present work, the turbine operates in 10 min turbulent wind series at maximum thrust with and without the flap control. The excitation force in longitudinal and lateral directions is given by the harmonic function

$$F(t) = A \cdot \sin(\omega t) \tag{19}$$

Through a sweep of excitation frequencies ω , the controller is tested by exciting the tower top in longitudinal and lateral directions.

13. RESULTS AND DISCUSSION

A stiff rotor in an aerodynamic quasi-steady fully attached flow [equations (11)–(15)] is compared to computations performed in HAWC2 with similar aerodynamic conditions, but without elastic deformation using constrained optimization. The parameters r_s , τ and K_p is free for the optimization algorithm, and r_f is traversed from 28 to 60 m. Figure 4 illustrates a good agreement between the time marching simulations in HAWC2 subjected to the described optimization strategy and equations (11)–(15). Both methods suggest placing the flap close to the blade tip at 59 m. The example is primarily used to validate that fatigue loads are calculated correctly and minimized by the optimization engine using the available free parameters; furthermore, despite the non-convex nature of the full constrained optimization problem, the found solution compares well with equation (15) (see Figure 4).

Elasticity, full aerodynamics and turbulent inflow are introduced in the second investigation. The aim was to find the sensor and flap position along the blade which gives the highest fatigue load reduction measured in the blade

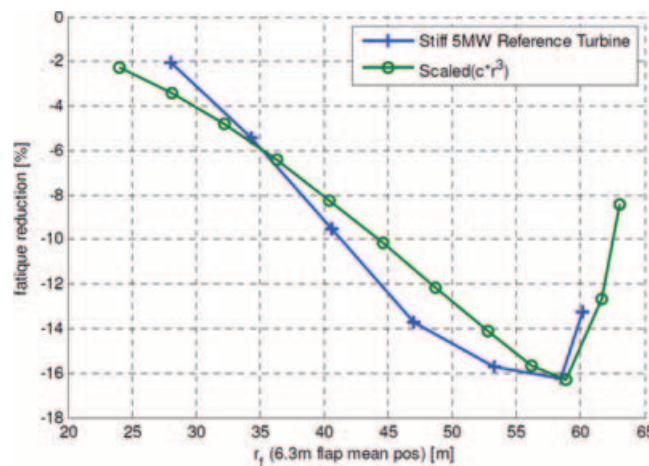


Figure 4. Flapwise root moment fatigue reductions as function of mean flap radial position.

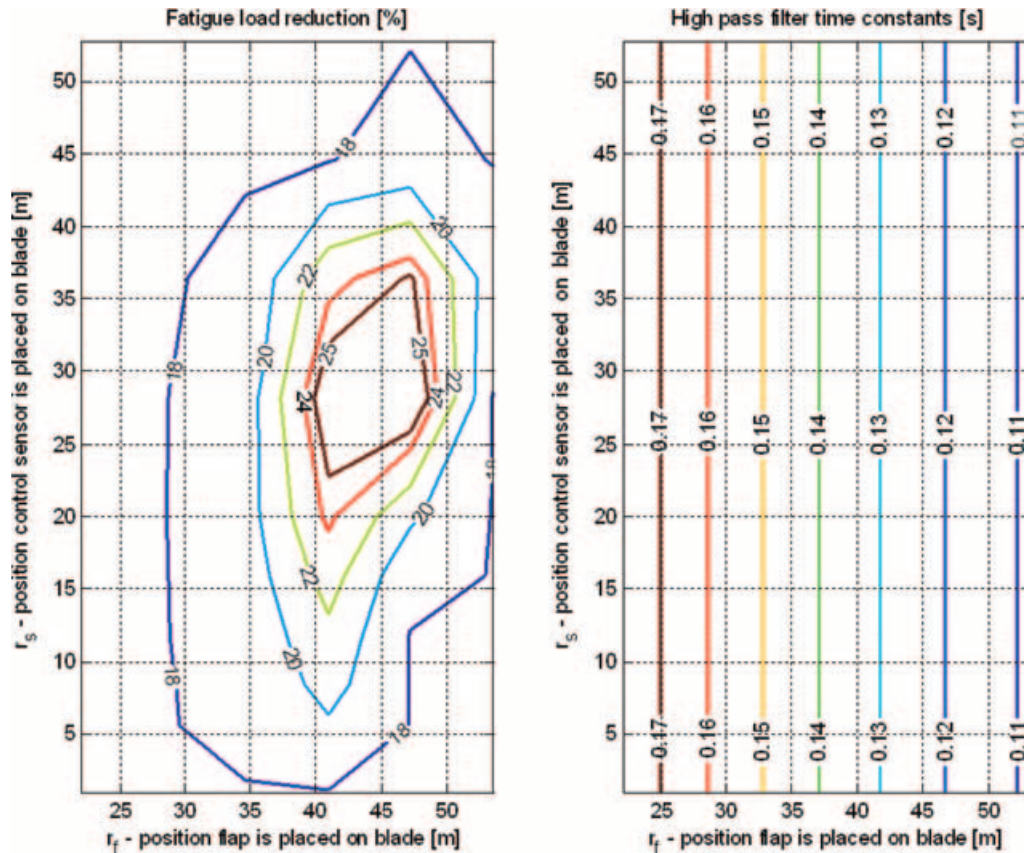


Figure 5. (Left) fatigue load reduction as function of control sensor and flap position; (right) high-frequency filter time constant from equation (10).

root bending moment. Figure 5 illustrates a parameter sweep of r_f and r_s while optimizing K_p . The filter time constant is set to a constant value specified in equation (10), which in general is slightly above the first flapwise eigenfrequency. According to Figure 5, the flap should be mounted 42–48 m from the blade root, and the strain gauge sensor should be placed 28 m from the blade root. It is important to realize that placing the control sensor near the blade root will not yield the highest fatigue load reductions, because the high-frequency pass filter have been given a constant value, equation (10), for all sensor positions. It is well known that a particular mode shape has a corresponding eigenfrequency. This leads to two possibilities when designing what dynamics should be captured by the sensor, either by moving the sensor along the blade or by adjusting the high-frequency pass filter time constant.

This leads to the third investigation, similar to the prior, with the exception that the high-frequency pass filter time constant τ is subjected to optimization. Figure 6 illustrates a parameter sweep of r_f and r_s , while optimizing K_p and τ . When comparing Figures 5 and 6, three features are distinctive; when optimizing τ , it becomes an intricate func-

tion of both r_f and r_s ; the control sensor near the blade root moment gives high load reductions, the high fatigue load reductions is no longer restricted to a narrow region near the center of the blade. Naturally, not all time constants are valid and not all sensor positions yield good results; in fact, only two sensor regions (blade root and around the center of the blade) offer high load reductions; however, there seems to be some flexibility when choosing sensor position and time constant. The optimization tends to place the sensor closer toward the blade root, when large time constants are used. As the time constant increase the frequency, band is widened allowing more low-frequency content in the input signal. An additional figure has been added (Figure 7) showing the standard deviation of flap deflection. The flap activity diminishes near the blade root region when using tuned filter time constants; this is an interesting bonus and not part of the optimization objective. It is not surprising that the flap deflection amplitude increases, thus the standard deviation, near the blade root because the normal force is proportional the relative wind speed squared, but it is perhaps surprising to see just how complex the relation between the best performing filter time constant and r_f , r_s is in Figure 6.

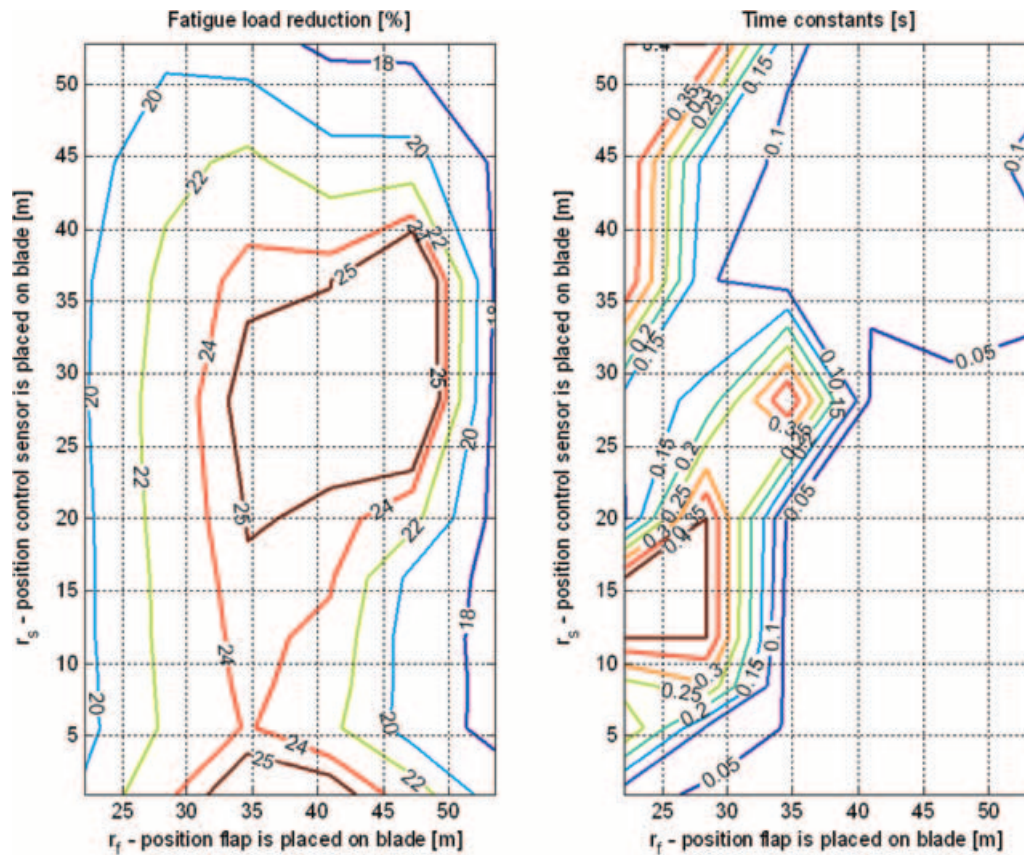


Figure 6. (Left) fatigue load reduction as function of control sensor and flap position; (right) optimized high-frequency filter time constant.

The flap position on the wind turbine blade giving the highest fatigue load reduction is investigated. Structurally elastic blades in flapwise, edgewise and torsional directions, and fully stiff blades were used. For the stiff blade, the flap should be placed 59 m from the blade root (see Figure 4); for the fully elastic blade, it dropped to 45 m (see Figure 5); if filter time constants became a free optimization parameter 48 m (see Figure 6). The flap mounted on the stiff blade reduced the blade root moment fatigue by 17%, and for the fully elastic blade the reduction was 25%. This is a perfect example of just how intricate the interdependencies are. The elastic part plays a significant role when assessing the fatigue load reduction potentials and should not be excluded, nor should the control parameters, or the interdependencies which clearly exist. This example serves as a warning that although the proposed controller is simple, the optimization problem is not; it is easy to lose overview of what goes on when the interdependencies come into play, for the more complex controllers like the class of model predictive controllers knowing what dynamics to exclude and how this will interact with the optimization problem is by no means trivial, but should nevertheless not be excluded in the design phase.

An intuitive subsequent step after mounting one flap on a wind turbine blade is to investigate the effect of having multiple flaps per blade instead. Initial investigations³³ revealed that additional flaps gave a decrease in fatigue loads. Two and three flaps per blade with corresponding strain gauge sensors were investigated, keeping the same setup as for the single flap per blade. For two flaps per blade, the optimization needed to tune 2×4 parameters, more specifically each of the two flaps needed to tune the position of the control sensor, the flap itself, the filtered time constant and the gain. For three flaps per blade, 3×4 parameters needed to be tuned, again with the same number of parameters per blade. The first thing to notice is the fact that although one flap gives a 25% fatigue load reduction, two flaps are far from giving 50%, in fact 'only' 34% is accomplished. Finally, adding the third flap per blade seems to yield even less in terms of fatigue load reduction. Table I gives an overview of the set of gains, time constants, flap and control sensor blade positions, yielding the highest fatigue load reductions in the flapwise blade root bending moment. The flap activity levels needed to facilitate these reductions are also part of the table and can be seen as the standard deviation in flap deflection row. Although the loads are not significantly decreased when

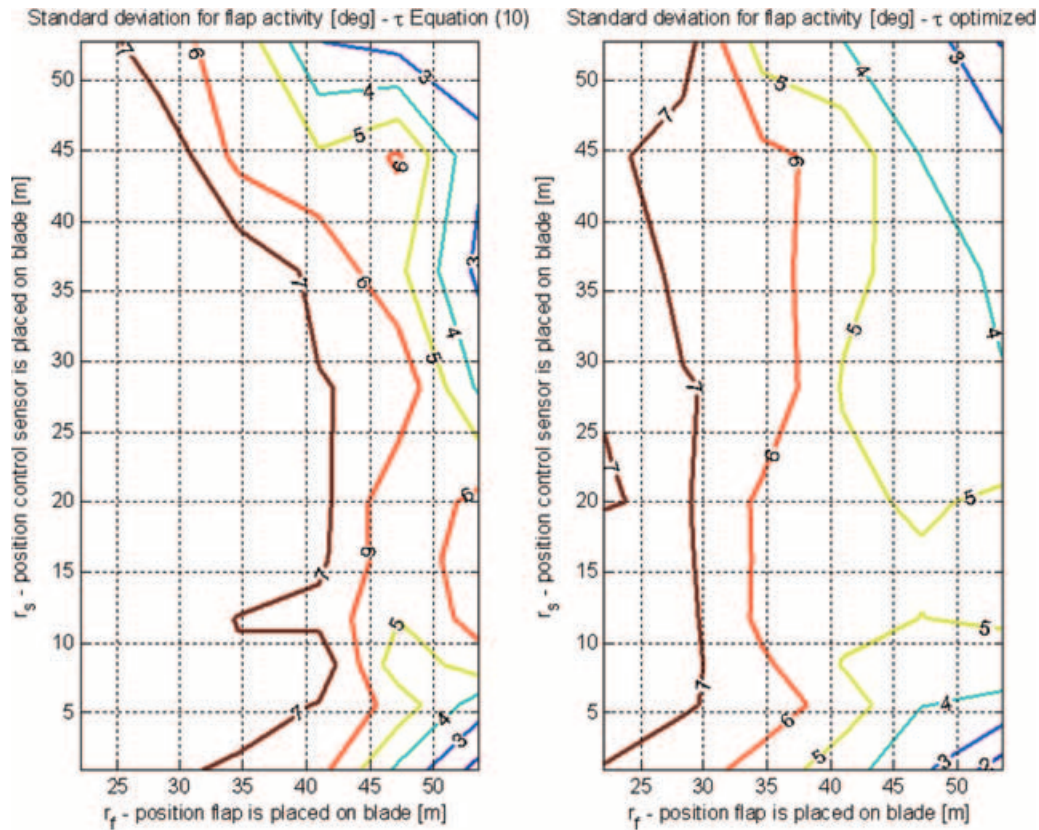


Figure 7. Flap activity illustrated using the standard deviation of the flap deflection signal from blade 1.

Table I. Flapwise root moment fatigue load reduction potential; where to place actuators and sensors, gain and time constants for one, two and three flaps mounted on a wind turbine blade.

	One flap (6.3 m)	Two flaps per blade (12.6 m)		Three flaps per blade (18.9 m)		
	1	1	2	1	2	3
Mean flap pos r_f (m)	45	34	45	30	45	54
Sensor pos r_s (m)	28	20	28	20	28	36
K_f (deg·KN m^{-1})/ τ (s)	0.044/0.05	0.071/0.32	0.032/0.04	0.060/0.35	0.034/0.10	0.025/0.03
Standard deviation flap deflection (deg)	4.9	4.2	3.8	3.7	3.4	2.1
Fatigue reduction (%)	25	34		37		

using three flaps per blade instead of one, the flap activity level is decreased, which could be useful knowledge for future smart rotor blade designs.

Although it becomes a huge parameter optimization problem, the optimization successfully converged to the results shown in Table I; however, the level of complexity and possible parameter combinations when applying more flaps increase tremendously.

However, the parameter space used during optimization of three flaps per blade can be reduced from 12 to 4 free parameters, if each new flap can be added and optimized independently from the previous. This has been investigated by means of the following iterative approach:

- Add flap 1, 2 and 3 on each blade.
- Tune flap 1 parameters.
- Tune flap 2 parameters.
- Tune flap 3 parameters.
- Repeat the second step until no more load reduction is possible.

The iterative approach for three flaps per blade was attempted, and load reductions per iteration are shown in Figure 8. Already after the first iteration cycle, where each of the flaps were tuned in sequence, the obtained load reduction is close to the result obtained using the full 12 free parameter optimization; naturally, this couples with

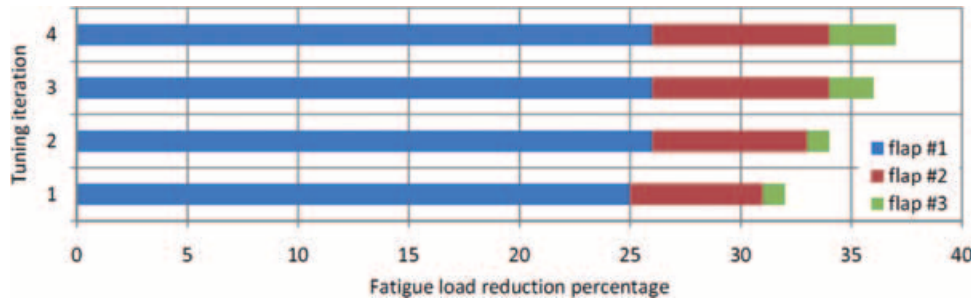


Figure 8. Fatigue load reduction percentage broken down per iteration and tuned flap.

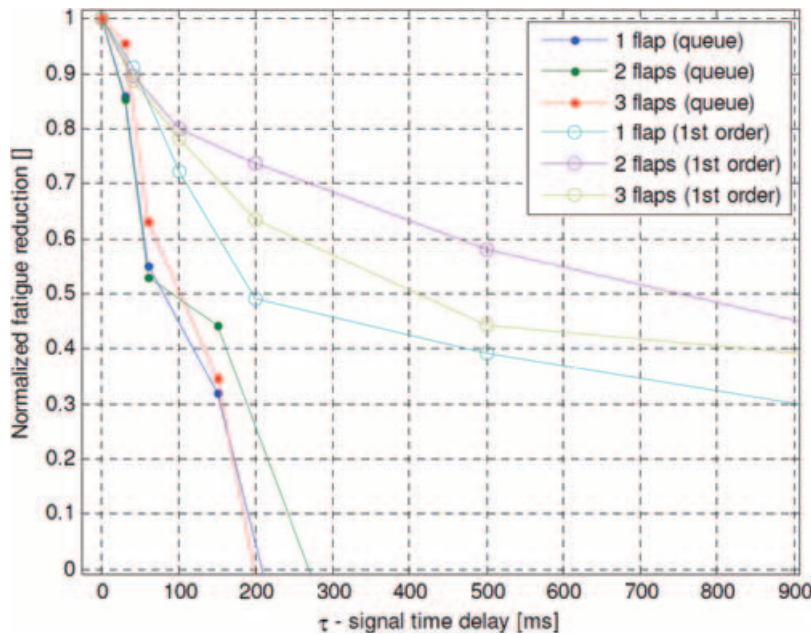


Figure 9. Load reduction affected by signal delay (queue style) and first-order signal lag.

well-suited starting guesses. It seems viable to reduce the optimization problem from 12 to 4 free parameters in this manner, especially because iterations 3 and 4 in Figure 8 compare well with the results from Table I, which is based on all 12 free parameters.

The effect of having additional delays in the control signal was also investigated. For fairness sake, it should be noted that no attempt was made to re-optimize the controller after signal delays and lags were introduced. According to Figure 9, the proposed controller is more sensitive to a signal delay than a signal lag. For the delayed signal, the flaps have no effect after 200 ms; typically, delays in signals originate from hardware, and 200 ms is substantial in this context. The same drastic reduction of the load reduction potential is not seen for the signal lag, in which the signal delay is modeled as a first-order filter. What remains to be investigated is the effect of having a differential term and more far reaching designing the con-

troller to react to the aerodynamic input in the form of a pitot tube or such rather than the elastic response in the form of a simulated strain measurement.

When using strain gauges or other types of gauges, the effect of signal noise will play a role in the performance of the controller. The effect of adding signal noise to the control signal has been investigated. The definition of the signal noise is provided in the previous chapter with all the model descriptions. In Figure 10, the fatigue load reduction is shown as function of the SNR; more specifically, the 1, 2, 3, 4, 5 and 10 dB ratios have been investigated, where 10 dB is the least affected signal and 1 dB the most deteriorated signal. Please note that the 49 dB shown in Figure 10 correspond to $SNR = \infty$ or in practice an unaffected signal. The investigation shows that once the SNR drops below 3 dB, the reduction potential starts deteriorating significantly; furthermore, if SNR is below 1 dB, the flaps should not be used with the present controller.

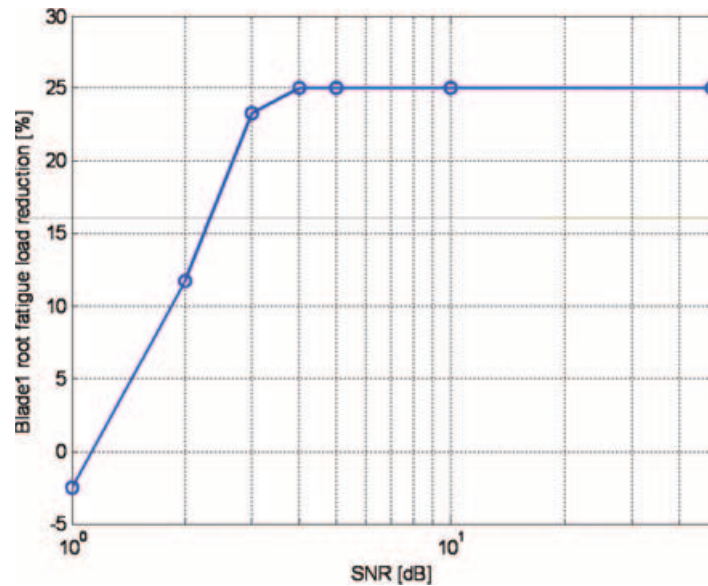


Figure 10. Effects of signal noise to the fatigue load reduction using the single flap per blade configuration.

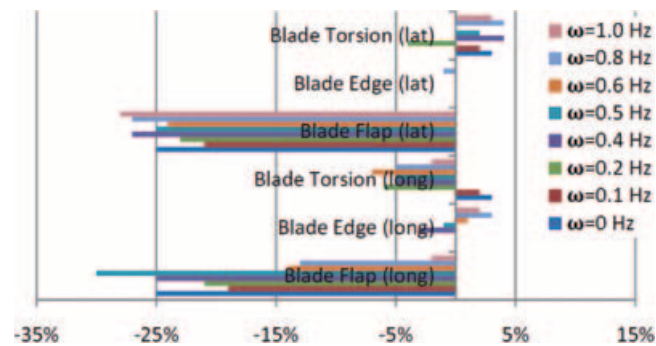


Figure 11. Blade root fatigue loads with harmonic tower top excitation in lateral (lat) and longitudinal (long) direction.

Although this is a crude investigation and the noise remains to be combined with, e.g. signal delays, typical SNR for strain gauges is well above 3 dB, which suggests that a signal noise investigation for this type of controller could be a second priority. The controller was not re-optimized after adding the white noise; thus, the best performing controller parameters pertaining to the undisturbed signal were kept for cases of signal lag and delay.

An important part of implementing a new controller is to predict possible instabilities. Fatigue numbers in blade, tower and drivetrain for 10 min turbulent wind series will be key performance indicators during the following somewhat crude stability analysis. The proposed controller has no information about the wind turbine or its surroundings besides the strain gauge sensor reading. It would be far easier to predict damping, if the control algorithm included all available states, from the tooth in the gear box, to the smallest eddy in the far wake; however, this is not possible

with the proposed setup. Although the present controller does not present an ideal setup for locating instabilities, harmonic excitations of the tower top with frequencies ranging from 0.1 to 1.0 Hz are used in an attempt to uncover possible stability issues. The additional 0 Hz excitation frequency corresponds to the standard case where the turbine only is excited by turbulent wind and inertial loads. In Figure 11, positive values indicate that the proposed flap controller performs worse than the baseline, which is a standard collective pitch variable-speed power controller without flaps. Negative values indicate an additional fatigue load reduction percentage compared to the variable-speed collective pitch controller. However, it should be noted that no instabilities were seen during these excitation runs.

The flapwise blade root fatigue loads are decreased significantly when the tower is excited in lateral and longitudinal directions, the edgewise blade root fatigue loads

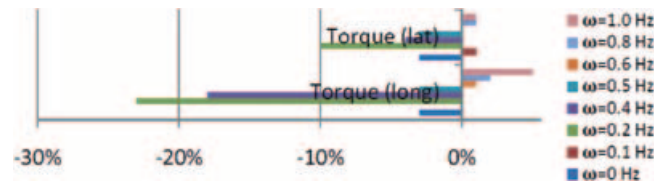


Figure 12. Torque fatigue loads with harmonic tower top excitation in lateral (lat) and longitudinal (long) direction.

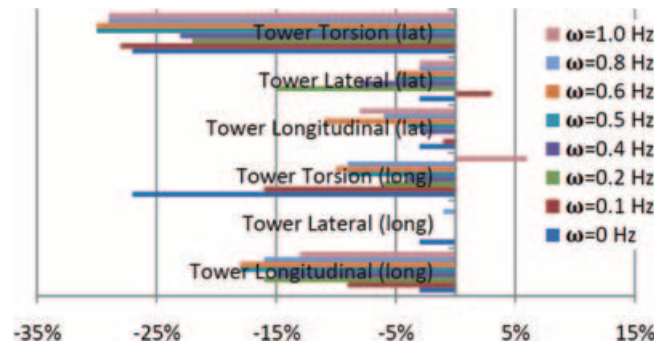


Figure 13. Tower root fatigue loads with harmonic tower top excitation in lateral (lat) and longitudinal (long) direction.

are nearly unchanged. A slight increase in torsional and torque fatigue loads at tower excitation frequencies 0.6, 0.8 and 1.0 Hz, is seen in Figure 12. Significant fatigue load reductions in root tower bending moment are shown in Figure 13. It is undesirable that torque and blade torsion fatigue loads increase, prior studies [3–11] reported that the significant decreases in lift fluctuations came at a price of increased torsional activity, but overall it may not be that important, and the proposed method for determining instabilities using a time marching code is very crude; however, these side effects could possibly be taken into account in a future smart rotor blade design. It should be noted that the controller presented in this work has been tested in offshore wind park simulations,³⁴ meandering turbulent wakes from one or several upstream turbines in direct or yawed conditions,³⁴ gusts following the IEC standard, and although the focus in the present study uses wind speeds close to rated power, in which the rotor thrust is the greatest, other control regions did not reveal instabilities.

An interesting investigation to be made as future work is a comparison between the simple control proposed in the current work and more advanced control models.

14. CONCLUSION

In the present work, a control algorithm for trailing edge flap has been proposed. The presented work utilizes the full aeroservoelastic multi-body model HAWC2¹⁸ as a component in the control loop design, offering the full

pallet of parameters for the optimization routine. A strain gauge sensor mounted on the blade in flapwise direction is used as input for the flap control. The computations are done on the 5 MW reference turbine¹⁷ used also in the EU-project ‘UpWind’. The flap comes in a standard length of 6.3 m, which is 10% of the overall blade length; when adding two flaps per blade, 20% of the overall blade length will be flapping and so forth.

Simple approximate considerations for a stiff rotor is formulated; based on the results from these considerations, the proposed setup comprising the closed loop controller, HAWC2, the constrained optimization engine and the simplified yet intricate interdependencies is tested while looking for the best place to attach a flap on a wind turbine blade. Both the approximate derivations and the full setup gave comparable results, indicating a success for the optimization in terms of finding the minima despite the non-convex nature of the optimization problem. For the reference turbine with blades stiff in flapwise, edgewise and torsional directions, the flap should be placed 59 m ($r/R = 0.94$) near the blade tip.

The optimum position for a flap was investigated using blades structurally elastic in flapwise, edgewise and torsional directions. For the stiff blade, the flap should be placed 59 m from the blade root; for the fully elastic blade, it dropped to 45 m. The strains should be measured 28 m from the blade root. The flap mounted on the stiff blade reduced the blade root moment fatigue by 17%; for the fully elastic blade, the reduction was 25%. The elastic part plays a significant role when using these tools to assess fatigue reduction potentials and when evaluating control designs.

When using optimization routines, it is important to have well-suited starting guesses. Based on numerous parameter sweeps, equation (9) for proportional gains is proposed and equation (10) for residual time constants. The equations should be regarded as suggestions for coming up with well-suited start guess for an optimization routine rather than actual equations rooted in physics.

The effect of placing two and three flaps per blade has been investigated; one flap can reduce the blade root moment fatigue load by 25%, two flaps 34% and three flaps 37%.

The effect of adding time lags and time delays in the control signal has been investigated. When a first-order time lag is introduced, the load reduction potential dropped to 50% after a 200 ms lag; it is not unrealistic to have lag of this magnitude in a closed loop flap controller.³⁵ On the other hand, a time delay (queue) of 200 ms is unrealistically huge, but investigated for the sake of completeness; a control signal put in a queue of 200 ms will render the flap(s) useless, and above 200 ms even harmful for the wind turbine.

Signal noise was investigated, which seemed to have an effect if the signal to white noise ratio deteriorates below 3 dB.

A crude stability analysis was carried out which involved exciting the turbine tower with a harmonically oscillating force at the top, and then searching for instability issues in the sensors. No instabilities were seen using this approach; however, the present controller with all the components in play does not present an ideal setup for locating instabilities. For the blade root, there is a slight increase in torsional fatigue loads and a significant decrease in flapwise fatigue loads when the tower is harmonically excited and the proposed flap controller is used. The torque fatigue loads also increase slightly for the tower excitation frequencies 0.6, 0.8 and 1.0 Hz.

Load reductions of 25–37% are not significantly better than what have been obtained using individual blade pitch, where 25% has been reported; however, the trailing edge flaps react to the elastic response only. Larger load reductions (45%) have been obtained when the flaps react to the aerodynamic input in the form of a pitot tube.⁸ (Andersen PB, Henriksen LC, Gaunaa M, Bak C, Buhl T. Deformable trailing edge flaps for modern mega-watt wind turbine controllers using pitot tubes. Unpublished)

An interesting investigation to be made as future work is a comparison between the simple control proposed in the current work and more advanced control models.

REFERENCES

1. Larsen TJ, Madsen HA, Thomsen K. Active load reduction using individual pitch, based on local blade flow measurements. *Wind Energy* 2004; **8**: 67–80.
2. Bossanyi EA. Developments in individual blade pitch control. *Wind Energy* 2003; **6**: 229–244.
3. Andersen PB, Gaunaa M, Bak C, Hansen MH. A dynamic stall model for airfoils with deformable trailing edges. *Wind Energy* 2009; **12**(8): 734–751.
4. Basualdo S. Load alleviation on wind turbine blades using variable airfoil geometry. *Wind Engineering* 2005; **29**(2): 169–182.
5. Trolborg N. Computational study of the Risø-B1-18 airfoil with a hinged flap providing variable trailing edge geometry. *Wind Engineering* 2005; **29**: 2005.
6. Buhl T, Gaunaa M, Bak C. Potential load reduction using airfoils with variable trailing edge geometry. *Journal of Solar Energy Engineering* 2005; **127**: 503–516.
7. Gaunaa M. The unsteady 2D potential-flow forces on a variable geometry airfoil undergoing arbitrary motion. *Risø-R-1478* 2006.
8. Andersen PB, Henriksen LC, Gaunaa M, Bak C, Buhl T. Integrating deformable trailing edge geometry in modern mega-watt wind turbine controllers. *European Wind Energy Conference and Exhibition, Brussels, Scientific proceedings*, 2008; 15–21.
9. Abdallah I. Advanced load alleviation for wind turbines using adaptive trailing edge geometry: sensing techniques. MSc Thesis, Department of Mechanical Engineering, Section of Fluid Mechanics, Technical University of Denmark, 2006.
10. Bak C, Gaunaa M, Andersen PB, Buhl T, Hansen P, Clemmensen K, Møller R. Wind tunnel test on wind turbine airfoil with adaptive trailing edge geometry. *[Technical Papers] Presented at the 42 AIAA Aerospace Sciences Meeting and Exhibit 45 AIAA Aerospace Sciences Meeting and Exhibit*, Reno, NV, 2007; 1–16.
11. Buhl T, Andersen PB. Deformable trailing edge geometries and cyclic pitch controller. *Sandia Blade Workshop*, Albuquerque, NM, 2008; 1–29.
12. Barlas T, van Kuik GAM. State of the art and perspectives of smart rotor control for wind turbines. *Journal of Physics* 2007; **5**. *2nd EWEA, EAWE The Science of Making Torque from Wind Conference*, Lyngby, 2007; 1–20.
13. van Wingerden JW, Huls Kamp AW, Barlas T, Marrant B, van Kuik GAM, Molenaar DP, Verhaegen M. On the proof of concept of a ‘smart’ wind turbine rotor blade for load alleviation. *Wind Energy* 2008; **11**: 265–280.
14. van Dam CP, Chow R, Zayas JR, Berg DA. Computational investigations of small deploying tabs and flaps for aerodynamic load control. *Journal of Physics* 2007; **5**. *2nd EWEA, EAWE The Science of Making Torque from Wind Conference*, Lyngby, 2007; 1–10.

15. Riziotis VA, Voutsinas SG. Aero-elastic modelling of the active flap concept for load control. *Proceedings (Online). 2008 European Wind Energy Conference and Exhibition*, Brussels, 2008; 1–9.
16. Troldborg N. Computational study of the Risø-B1-18 airfoil equipped with active controlled trailing edge flaps. Master Thesis, Department of Mechanical Engineering, Fluid Mechanics, Technical University of Denmark, 2004.
17. Jonkman J. NREL 5 MW baseline wind turbine. *Technical Report*, NREL/NWTC, 1617 Cole Boulevard; Golden, CO 80401-3393, 2005.
18. Larsen TJ, Hansen AM. Influence of blade pitch loads by large blade deflections and pitch actuator dynamics using the new aeroelastic code HAWC2. *Paper and Oral Presentation at EWEC*, Athens, 2006; 1–5.
19. Theodorsen T. General theory of aerodynamical instability and the mechanism of flutter. *NACA Report* 496, 1935.
20. Leishman JG. Unsteady lift of a flapped airfoil by indicial concepts. *Journal of Aircraft* 1994; **31**: 288–297.
21. Hariharan N, Leishman JG. Unsteady aerodynamics of a flapped airfoil in subsonic flow by indicial concepts. *Journal of Aircraft* 1996; **33**: 855–868.
22. Katz J, Weihs D. The effect of chordwise flexibility on the lift of a rapidly accelerated airfoil. *Aeronautical Quarterly* 1979; **30**: 360–370.
23. van der Wall BG, Geissler W. Experimental and numerical investigations on steady and unsteady behaviour of a rotor airfoil with a piezoelectric trailing edge flap. *55th American Helicopter Society Forum*, Montreal, 1999; 963–976.
24. Andersen PB, Gaunaa M, Bak C, Hansen MH. Implementing a dynamic stall model for airfoils with deformable trailing edges. *46th AIAA Aerospace Sciences Meeting and Exhibit*, Reno, NV, 2008; 1328.
25. Hansen MH, Gaunaa M, Madsen AM. A Beddoes–Leishman type dynamic stall model in state-space and indicial formulation. *Risø-R-Report, Risø-R-1354(EN), Risø National Lab.*, Roskilde, 2004; 1–40.
26. Leishman JG, Beddoes TS. A generalized model for airfoil unsteady aerodynamic behavior and dynamic stall using indicial method. *Proceedings of the 42nd Annual Forum of the American Helicopter Society*, Washington DC, 1986; 243–266.
27. Beddoes TS. A near wake dynamic model. *Aerodynamics and Aeroacoustics National Specialist Meeting. Papers and Discussion*, 1987.
28. Madsen HA, Rasmussen F. A near wake model for trailing vorticity compared with the blade element momentum theory. *Wind Energy* 2004; **7**: 325–341.
29. Andersen PB, Gaunaa M, Madsen MH. A near wake model with far wake effects implemented in a multi body aero-servo-elastic code. *Wind Energy* (In press).
30. Sørensen NN, Madsen HA. Modelling of transient wind turbine loads during pitch motion. *Proceedings (Online). 2006 European Wind Energy Conference and Exhibition*, Athens, 2006; 1–10.
31. Wilson RE, Lissaman PBS. *Applied Aerodynamics of Wind Power Machines*. Oregon State University: Corvallis, 1974.
32. Reveliotis S. An introduction to linear programming and the simplex algorithm. Georgia Institute of Technology. [Online]. Available: <http://www2.isye.gatech.edu/~spyros/LP/LP.html>. (Accessed 20 November 2009)
33. Andersen PB, Gaunaa M, Bak C, Buhl T. Load alleviation on wind turbine blades using variable airfoil geometry. *Proceedings (Online). 2006 European Wind Energy Conference and Exhibition*, Athens, 2006; 8.
34. Markov H, Andersen PB, Larsen G. *Potential of Trailing Edges Flaps Exposed to Wakes Emitted from Upstream Modern Megawatt Turbines*. Euromech Colloquium in Madrid: Madrid, 2009.
35. Andersen PB, Bak C, Gaunaa M, Buhl T. Wind tunnel test on wind turbine airfoil with closed loop controller for adaptive trailing edge flap. *Risoe-R-1707*, ISBN:978-87-550-3773-1.